

Fixed-Time Newton-Like Extremum Seeking

J. I. Poveda* M. Krstić**

* *Department of Electrical, Computer, and Energy Engineering, University of Colorado, Boulder, CO 80309 USA (e-mail: jorge.poveda@colorado.edu).*

** *Department of Mechanical and Aerospace Engineering, University of California, San Diego, CA 92093 USA (e-mail: krstic@ucsd.edu).*

Abstract: In this paper, we present a novel Newton-based extremum seeking controller for the solution of multivariable model-free optimization problems in static maps. Unlike existing asymptotic and fixed-time results in the literature, we present a scheme that achieves (practical) finite time convergence to a neighborhood of the optimal point, with a convergence time that is independent of the initial conditions and the Hessian of the cost function, and therefore can be arbitrarily assigned a priori by the designer with an appropriate choice of parameters in the algorithm. The extremum seeking dynamics exploit a class of fixed time convergence properties recently established in the literature for a family of Newton flows, as well as averaging results for perturbed dynamical systems that are not necessarily Lipschitz continuous. The proposed extremum seeking algorithm is model-free and does not require any explicit knowledge of the gradient and Hessian of the cost function. Instead, real-time optimization with fixed-time convergence is achieved by using real time measurements of the cost, which is perturbed by a suitable class of periodic excitation signals generated by a dynamic oscillator. Numerical examples illustrate the performance of the algorithm.

Keywords: Extremum seeking, adaptive control, optimization.

1. INTRODUCTION

In several applications it is of interest to recursively minimize a particular cost function whose mathematical form is unknown and which is only accessible via measurements. For these types of problems, extremum seeking (ES) algorithms have shown to be a powerful technique with provable stability, convergence, and robustness guarantees; see for instance Ariyur and Krstić (2003); Tan et al. (2006); Nešić et al. (2010); Grushkovskaya et al. (2017); Oliveira et al. (2017); Suttner (2019); Guay and Zhang (2003); Teel and Popovic (2001) and Poveda and Teel (2017) for different extremum seeking architectures, applications, and theoretical results. Recently, there has been growing interest in improving the transient performance of ES algorithms by accelerating the rate of convergence. This has motivated the development in (Poveda and Teel, 2017, Sec. 6.1) of discontinuous algorithms, accelerated hybrid ES dynamics presented in Poveda and Li (2021), as well as multivariable Newton-based schemes with an exponential rate of convergence that can be assigned a priori by the practitioner, see Ghaffari et al. (2012). Nevertheless, while these schemes exhibit better transient performance compared to the traditional gradient descent-based schemes, the convergence time is still highly dependent on the initial conditions of the algorithm.

On the other hand, there has been a lot of recent efforts in designing control, estimation, and optimization algorithms with non-asymptotic convergence properties. These algo-

gorithms guarantee convergence to the desired target in a finite time that is independent of the initial conditions, see for instance Cruz-Zavala et al. (2010); Engel and Kreiselmeyer (2002); Polyakov (2012); Andrieu et al. (2008); Garg and Panagou (2018); Polyakov (2012) and Romero and Benosman (2019). These results have opened the door to novel dynamical systems that are able to achieve fixed-time convergence using discontinuous or continuous vector fields; see for instance Li et al. (2017) and Garg and Panagou (2018). Such results have also recently motivated a gradient-based ES algorithms with fixed-time convergence properties, presented in Poveda and Krstić (2020a), where for the convex case the upper bound on the convergence time was shown to be independent of the initial conditions, but dependent on the smallest eigenvalue of the Hessian of the cost function, see (Poveda and Krstić, 2020a, Remark 1).

Motivated by this background, in this paper we present a novel Newton-based ES algorithm with fixed-time (practical) convergence properties, where the upper bound on the convergence time is now independent of the Hessian, and therefore can be arbitrarily assigned by the designer with a suitable choice of parameters in the algorithm. Our results are inspired by the previous architectures of Newton-based ES with asymptotic properties presented in Ghaffari et al. (2012) and Ghaffari et al. (2014), as well as by the recent model-based Newton-flows with fixed-time convergence properties introduced in Garg and Panagou (2018). In particular, we show that, under a suitable modification of the vector field used in standard multivariable Newton-based ES, fixed-time practical convergence can be achieved. Given that Newton-based ES dynamics

* Research supported in part by CU Boulder - Autonomous Systems IRT Seed Grant No. 11005946, and NSF grants 1823983 & 1711373.

and

$$\dot{\xi}_2 = F_{\xi_2}(\xi, x, \mu) := \frac{1}{\varepsilon_2} \left(-\xi_2 + \phi(z)M(\mu) \right), \quad (7)$$

where $\varepsilon_2 \in \mathbb{R}_{>0}$ is a tunable parameter selected sufficiently small to guarantee that (6) and (7) evolve in a faster time scale compared to the dynamics (4). As shown in the next section, the state ξ_1 can be seen as an estimation of the inverse of the Hessian matrix $\nabla^2\phi(x)$, while the state ξ_2 can be seen as an estimation of the gradient $\nabla\phi(x)$.

In system (6)-(7), the state μ is generated by a constrained linear oscillator evolving on \mathbb{T}^n , given by:

$$\dot{\mu} = \frac{2\pi}{\varepsilon_1} \mathcal{R}_\theta \mu, \quad \mu \in \mathbb{T}^n, \quad (8)$$

where the parameter $\varepsilon_1 > 0$ is selected sufficiently small to guarantee that the dynamics (8) operate in a faster time scale compared to the dynamics (4), (6), and (7), i.e., $\varepsilon_1 \ll \varepsilon_2$. In order to guarantee that (8) is a dynamic oscillator, we define the matrix $\mathcal{R}_\theta \in \mathbb{R}^{2n \times 2n}$ as a block diagonal matrix with blocks $\mathbf{R}_i \in \mathbb{R}^{2 \times 2}$ defined as

$$\mathbf{R}_i := \begin{bmatrix} 0 & \theta_i \\ -\theta_i & 0 \end{bmatrix}, \quad \theta_i \in \mathbb{R}_{>0}.$$

To link the states (x, μ) , generated by the dynamics (4) and (8), to the argument of the cost function $\phi(z)$, we set the argument z via the feedback law

$$z := x + a\tilde{\mu}, \quad (9)$$

where $a \in \mathbb{R}_{>0}$ is a tunable parameter, and where $\tilde{\mu} \in \mathbb{R}^n$ is the vector that contains the odd entries of $\mu \in \mathbb{R}^{2n}$, i.e.,

$$\tilde{\mu} := [\mu_1, \mu_3, \mu_5, \dots, \mu_{2n-1}]^\top. \quad (10)$$

Note that $\tilde{\mu}$ can be written as $\tilde{\mu} = \mathcal{D}\mu$, with $\mathcal{D} \in \mathbb{R}^{n \times 2n}$ being a suitable matrix with entries $\mathcal{D}_{i,j} \in \{0, 1\}$.

The gradient and Hessian estimators (6)-(7) depend on the excitation functions $N : \mathbb{R}^{2n} \rightarrow \mathbb{R}^{n \times n}$ and $M : \mathbb{R}^{2n} \rightarrow \mathbb{R}^n$, which are defined as

$$M(\mu) := \frac{2}{a} \mathcal{D}\mu, \quad N(\mu) := \begin{bmatrix} N_{11} & N_{12} & \dots & N_{1n} \\ N_{21} & N_{22} & \dots & N_{2n} \\ \vdots & \vdots & \vdots & \vdots \\ N_{n1} & N_{n2} & \dots & N_{nn} \end{bmatrix}, \quad (11)$$

where the entries N_{ij} satisfy $N_{ij} = N_{ji}$, as well as the conditions:

$$N_{ij} = \frac{16}{a^2} \left(\tilde{\mu}_i^2 - \frac{1}{2} \right), \quad \forall i = j, \quad (12a)$$

$$N_{ij} = \frac{4}{a^2} \tilde{\mu}_i \tilde{\mu}_j, \quad \forall i \neq j. \quad (12b)$$

As shown in the next section, under suitable choices of the parameters $(a, \varepsilon_1, \theta_i)$, the excitation signals (11) guarantee an estimation of order $O(a)$ of the Hessian $\nabla^2\phi(x)$ and the gradient $\nabla\phi(x)$ via the dynamics (6) and (7). Since a is a tunable parameter, the estimation error can be made arbitrarily small on compact sets.

Remark 2. The structure of the NFxTES is similar to the multi-variable Newton-based extremum seeking controller considered in Ghaffari et al. (2012). However, the NFxTES dynamics have two main differences: a) under suitable choices of the parameters (q_1, q_2) , the dynamics of x are continuous but not Lipschitz continuous, and they aim to approximate a Newton-based flow with fixed-time convergence properties instead of the Newton-based flow $\dot{x} = -\nabla^2\phi(x)^{-1}\nabla\phi(x)$ considered in Ghaffari et al. (2012);

b) the dither signals $N(\cdot)$, $M(\cdot)$ and $\tilde{\mu}(\cdot)$ are generated by the linear oscillator (8), which evolves on the torus \mathbb{T}^n . This allows us to analyze the NFxTES as a *time-invariant* dynamical system. \square

3.2 Main Result

In this section, we establish the main convergence properties of the NFxTES. In order to do this, we define the *admissible* parameters (q_1, q_2, k) as any tuple that satisfies the following relationships:

$$q_1 \in (2, \infty), \quad q_2 \in (1, 2), \quad k \in (0, \infty) \quad (13)$$

As shown in (Garg and Panagou, 2018, Lemma 6), an admissible tuple of parameters guarantees that $1 - \alpha_1 > 0$ and $1 - \alpha_2 > 0$. Therefore, we have that

$$\left| \lim_{\xi_2 \rightarrow 0} \frac{\xi_1 \xi_2}{|\xi_2|^{\alpha_1}} \right| \leq |\xi_1| \lim_{\xi_2 \rightarrow 0} |\xi_2|^{1-\alpha_1} = 0.$$

Using the same procedure for $\left| \frac{\xi_1 \xi_2}{|\xi_2|^{\alpha_2}} \right|$, one obtains that

$\left| \lim_{\xi_2 \rightarrow 0} \frac{\xi_1 \xi_2}{|\xi_2|^{\alpha_2}} \right| = 0$, which establishes continuity of the vector field (4) at points satisfying $\xi_2 = 0$. Continuity at points $\xi_2 \neq 0$ follows trivially by the structure of the dynamics. Based on this, we consider the following assumption on the parameters of the algorithm:

Assumption 3. The tuple of parameters (q_1, q_2, k) is admissible; and for each $i \in \{1, 2, \dots, n\}$ the parameter θ_i is a positive rational number, and $\theta_i \neq \theta_j$ for all $i \neq j$. \square

Remark 4. The second condition of Assumption 3 is standard in extremum seeking control, see for instance Nešić et al. (2010), Ghaffari et al. (2012), and Poveda and Teel (2017), and it facilitates the application of averaging theory to analyze the qualitative behavior of the extremum seeking dynamics. \square

For each admissible tuple of parameters (q_1, q_2, k) , we define the value

$$T^* := \frac{1}{k} \left[\left(\frac{2^{0.5\alpha_1}}{\alpha_1} \right) - \left(\frac{2^{0.5\alpha_2}}{\alpha_2} \right) \right], \quad (14)$$

where (α_1, α_2) are defined as in (5). Note that admissible parameters always guarantee that the term inside the brackets is positive. Thus, for each desired $T^* > 0$ one can always satisfy equation (14) by choosing admissible parameters (q_1, q_2, k) with

$$k = \frac{1}{T^*} \left[\left(\frac{2^{0.5\alpha_1}}{\alpha_1} \right) - \left(\frac{2^{0.5\alpha_2}}{\alpha_2} \right) \right]. \quad (15)$$

Using the definition of T^* in (14), and the NFxTES dynamics (4), (6), (7), and (8), we are now ready to state the main result of the paper. The complete proof is presented in Poveda and Krstić (2020b).

Theorem 5. Consider the NFxTES dynamics and suppose that Assumptions 1 and 3 hold. Then, for admissible parameters (q_1, q_2, k) and each $\nu > 0$ there exists $\varepsilon_2^* > 0$ such that for each $\varepsilon_2 \in (0, \varepsilon_2^*)$ there exists $a^* > 0$ such that for each $a \in (0, a^*)$ there exists $\varepsilon_1^* > 0$ such that for each $\varepsilon_1 \in (0, \varepsilon_1^*)$ there exists a neighborhood \mathcal{N} of $p^* := (z^*, \nabla^2\phi(z^*)^{-1}, \nabla\phi(z^*))$ such that every solution with $(x(0), \xi(0), \mu(0)) \in \mathcal{N} \times \mathbb{T}^n$ exists for all time, and satisfies

$$|x(t) - z^*| \leq \nu, \quad \forall t \geq T^*, \quad (16)$$

where T^* is given by (14). \square

While the convergence result of Theorem 5 is local with respect to the initial conditions, practical with respect to the parameters $(\varepsilon_1, \varepsilon_2, a)$ and the neighborhood $\{z^*\} + \nu\mathbb{B}$, and finite with respect to time, there is a key difference with respect to previous results in the literature of extremum seeking: the upper bound T^* on the convergence time is independent of the initial conditions and the Hessian of the cost function, and therefore can be arbitrarily assigned a priori by the designer using an appropriate choice of admissible parameters (q_1, q_2, k) , such as in (15). This represents a clear advantage even with respect to *gradient*-based fixed-time ES dynamics, e.g., Poveda and Krstić (2020a), where the value of T^* depends on the smallest eigenvalue of the Hessian matrix $\nabla^2\phi(z)$.

Sketch of the Proof of Theorem 5: We start with the following auxiliary Lemma:

Lemma 6. Suppose that Assumption 3 holds and consider the linear oscillator (8) with $\varepsilon_1 = 1$ and the signal $\tilde{\mu}$ defined in (10). Then, there exists a $T > 0$ such that for all solutions μ of (8) the following integrals hold:

$$\frac{1}{T} \int_0^T \tilde{\mu}_i(s) ds = 0, \quad \forall i \in \{1, 2, \dots, n\}. \quad (17a)$$

$$\frac{1}{T} \int_0^T \tilde{\mu}_i(s)^2 ds = \frac{1}{2}, \quad (17b)$$

$$\frac{1}{T} \int_0^T \tilde{\mu}_i(s) \tilde{\mu}_j(s) ds = 0, \quad \forall i \neq j, \quad (17c)$$

$$\frac{1}{T} \int_0^T \tilde{\mu}_i(s)^2 N_{ii}(s) ds = \frac{1}{8}, \quad \forall i \in \{1, 2, \dots, n\}, \quad (17d)$$

$$\frac{1}{T} \int_0^T \tilde{\mu}_i(s)^2 N_{jj}(s) ds = 0, \quad \forall i \neq j, \quad (17e)$$

$$\frac{1}{T} \int_0^T \tilde{\mu}_i(s)^2 N_{ij}(s) ds = 0, \quad \forall i \neq j, \quad (17f)$$

$$\frac{1}{T} \int_0^T \tilde{\mu}_i(s) N_{ij}(s) ds = 0, \quad \forall i \neq j, \quad (17g)$$

$$\frac{1}{T} \int_0^T \tilde{\mu}_i(s) N_{ii}(s) ds = 0, \quad \forall i \in \{1, 2, \dots, n\}, \quad (17h)$$

$$\frac{1}{T} \int_0^T \tilde{\mu}_i(s) N_{jj}(s) ds = 0, \quad \forall i \neq j, \quad (17i)$$

$$\frac{1}{T} \int_0^T \tilde{\mu}_i(s) \tilde{\mu}_j(s) N_{ij}(s) ds = \frac{1}{4}, \quad \forall i \neq j, \quad (17j)$$

$$\frac{1}{T} \int_0^T \tilde{\mu}_i(s) \tilde{\mu}_j(s) N_{ii}(s) ds = 0, \quad \forall i \neq j. \quad (17k)$$

□

Proof: The proof of Lemma 6 follows by taking $T = 2\pi \times \text{LCM}\{\frac{1}{\kappa_1}, \frac{1}{\kappa_2}, \dots, \frac{1}{\kappa_n}\}$, where LCM stands for the least common multiplier, and noticing that every solution $\tilde{\mu}_i$ generated by the oscillator (8) with $\varepsilon_1 = 1$ is of the form

$$\tilde{\mu}_i(t) = \mu_{i,1}(0) \cos(2\pi\kappa_i t) + \mu_{i,2}(0) \sin(2\pi\kappa_i t), \quad (18)$$

with $\mu_{i,1}(0)^2 + \mu_{i,2}(0)^2 = 1$. Using the expression (18) all the integrals of (17) follow by direct computation. ■

The properties of Lemma 6 allow us to obtain real-time gradient and Hessian estimations in (6) and (7) -on average- by using only measurements of the cost function $\phi(z)$. In particular, by taking a Taylor expansion of $\phi(x + a\tilde{\mu})$ around x for small values of a , we obtain:

$$\phi(x + a\tilde{\mu}) = \phi(x) + a\tilde{\mu}^\top \nabla\phi(x) + \frac{a^2}{2} \tilde{\mu}^\top \nabla^2\phi(x) \tilde{\mu} + O(a^3).$$

Using the definitions of $M(\cdot)$ and $N(\cdot)$, and the integrals (17), we obtain the following average functions, where the average is taken with respect to the solutions of the oscillator (8), i.e., keeping x constant:

$$\frac{1}{T} \int_0^T \phi(x + a\tilde{\mu}(s)) M(\mu(s)) ds = \nabla\phi(x) + O(a), \quad (19)$$

and

$$\frac{1}{T} \int_0^T \phi(x + a\tilde{\mu}(s)) N(\mu(s)) ds = \nabla^2\phi(x) + O(a), \quad (20)$$

which correspond to $O(a)$ -perturbed versions of the gradient and the Hessian of the cost function ϕ , with a perturbation that shrinks as $a \rightarrow 0^+$. Therefore, by computing the average of the dynamics (4), (6), and (7) along the solutions of (8), and by neglecting the $O(a)$ disturbance of (19) and (20), we can obtain the following average dynamics:

$$\dot{x} = F_x^A(\xi_1, \xi_2) := -\xi_1 \xi_2 \left(\frac{k}{\|\xi_2\|^{\alpha_1}} + \frac{k}{\|\xi_2\|^{\alpha_2}} \right), \quad (21a)$$

$$\dot{\xi}_1 = F_{\xi_1}^A(\xi, x) := \frac{1}{\varepsilon_2} \left(\xi_1 - \xi_1 \nabla^2\phi(x) \xi_1 \right), \quad (21b)$$

$$\dot{\xi}_2 = F_{\xi_2}^A(\xi, x) := \frac{1}{\varepsilon_2} \left(-\xi_2 + \nabla\phi(x) \right). \quad (21c)$$

When ε_2 is sufficiently small, system (21) is a singularly perturbed system. The boundary layer dynamics of this system can be obtained by setting $\dot{x} = 0$ and $\varepsilon_2 = 1$:

$$\dot{\xi}_1 = \xi_1 - \xi_1 \nabla^2\phi(x) \xi_1, \quad (22a)$$

$$\dot{\xi}_2 = -\xi_2 + \nabla\phi(x). \quad (22b)$$

For fixed values of x , the stability properties of system (22) can be analyzed as follows: denote by $r_x := \nabla\phi(x)$ and $H_x := \nabla^2\phi(x)$, and consider the errors $\tilde{\xi}_1 = \xi_1 - H_x^{-1}$ and $\tilde{\xi}_2 = \xi_2 - r_x$. The error boundary layer dynamics are then given by the following decoupled equations:

$$\dot{\tilde{\xi}}_1 = -\tilde{\xi}_1 H_x (\tilde{\xi}_1 + H_x^{-1}) \quad (23a)$$

$$\dot{\tilde{\xi}}_2 = -\tilde{\xi}_2. \quad (23b)$$

System (23b) has the origin globally exponentially stable, and system (23a) has the origin locally exponentially stable since its linearization around the origin has the Jacobian $-I$, see (Ghaffari et al., 2012, pp. 1761). Therefore, for each fixed x , the boundary layer dynamics render the quasi-steady state mapping

$$\xi^* = M(x) := (\nabla^2\phi(x)^{-1}, \nabla\phi(x)),$$

locally exponentially stable, uniformly on x .

The reduced dynamics associated to system (21) are obtained by substituting ξ^* in (21a):

$$\dot{x} = -k \nabla^2\phi(x)^{-1} \left(\frac{\nabla\phi(x)}{\|\nabla\phi(x)\|^{\alpha_1}} + \frac{\nabla\phi(x)}{\|\nabla\phi(x)\|^{\alpha_2}} \right). \quad (24)$$

Following the ideas of Garg and Panagou (2018), system (24) can be analyzed using the Lyapunov function

$$V(x) = \frac{1}{2} |\nabla\phi(x)|^2,$$

which under Assumption 1 is positive definite with respect to the point $\{z^*\}$, and also has bounded level sets. The derivative of V along the solutions of (24) is given by

$$\dot{V}(x) = -c_1 2^{\frac{\alpha_1}{2}} V(x)^{\frac{\alpha_1}{2}} - c_2 2^{\frac{\alpha_2}{2}} V(x)^{\frac{\alpha_2}{2}}, \quad (25)$$

which, by (Polyakov, 2012, Lemma 1), implies that the point $\{z^*\}$ is fixed-time stable. Thus, all solutions of (24) satisfy a bound of the form

$$|x(t) - z^*| \leq \beta_x(|x(0) - z^*|, t), \quad \forall t \geq 0,$$

where $\beta_x \in \mathcal{KL}_{\mathcal{T}}$, i.e., β is a \mathcal{KL} function that also satisfies the condition (Rios and Teel, 2018, Sec. 2.1) $\beta_x(r, t) = 0$, for all $t \geq T^*$ and $r \geq 0$, where T^* is given by (14). From here, the main result of the theorem follows by applying the averaging results of (Poveda and Li, 2021, Thm. 7) that preserves the \mathcal{KL} bound of the slow dynamics (24) for the evolution of the state x in the original dynamics (4). ■

Remark 7. The local nature of Theorem 5 is due to the existence of multiple equilibria in the dynamics

$$\dot{\xi}_1 = \left(\xi_1 - \xi_1 \nabla^2 \phi(z) \xi_1 \right), \quad (26)$$

which corresponds to the average dynamics of (6). Similar local results emerge in Newton-based ESCs with asymptotic convergence properties; see for instance Ghaffari et al. (2012). While it is possible to design Newton-based ESCs with semi-global practical asymptotic stability results by computing the vector $\nabla^2 \phi(x)^{-1} \nabla \phi(x)$ using the singular perturbation approach presented in (Alvarez et al., 2002, Sec. 3), said approach cannot be used in this case since it will generate dynamics (4) with discontinuous vector fields that are not locally bounded. □

4. NUMERICAL RESULTS

To illustrate the performance of the NFxTES, and to highlight the differences with respect to the standard Newton-based extremum seeking controller of Ghaffari et al. (2012), we consider the quadratic function

$$\phi(z) = \frac{1}{2} z^T H z + b^T z + c, \quad (27)$$

which satisfies $\nabla \phi(z) = H z + b$ and $\nabla^2 \phi(z) = H$. The parameters of (27) are selected as

$$H = \begin{bmatrix} 4 & 1 \\ 1 & 2 \end{bmatrix}, \quad b = \begin{bmatrix} -4 \\ -6 \end{bmatrix}, \quad c = 11.$$

The inverse of the Hessian matrix is given by

$$H^{-1} = \begin{bmatrix} 0.2857 & -0.1429 \\ -0.1429 & 0.5714 \end{bmatrix}, \quad (28)$$

and the function $\phi(z)$ has a global minimizer at the point

$$z^* = -H^{-1}b = \left[\frac{2}{7}, \frac{20}{7} \right]^T.$$

In order to find z^* in fixed time, we implement the NFxTES dynamics with parameters $a = 0.1$, $\varepsilon_1 = 0.1$ and $\varepsilon_2 = 10$. The constants (k, q_1, q_2) were selected as $k = 0.025$, $q_1 = 3$, and $q_2 = 1.5$, which generate an upper bound on the convergence time given by $T^* = 123.4$. We also simulate the Newton-based ES algorithm of Ghaffari et al. (2012), which has learning dynamics of the form $\dot{x} = -k\xi_1\xi_2$. To obtain a smooth approximation of H^{-1} , we have also implemented an additional low-pass filter that receives as input ξ_1 and ξ_2 and generates filtered outputs ξ_1^f and ξ_2^f that serve as inputs to the learning dynamics. As shown in Ghaffari et al. (2012), the incorporation of these filters does not affect the stability analysis of the algorithm. Figure 2 shows the trajectories generated

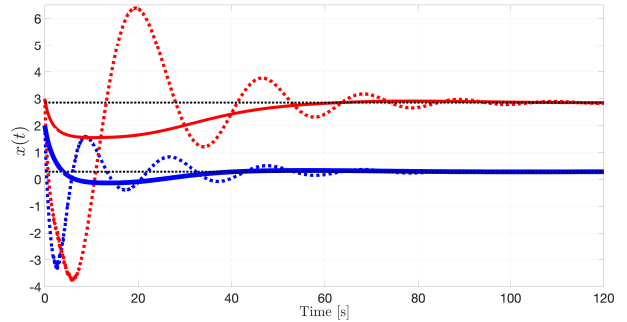


Fig. 2. Evolution in time of the state x . Blue line corresponds to x_1 , and red line corresponds to x_2 . The dotted lines correspond to the trajectories generated by the traditional Newton-based ESC of Ghaffari et al. (2012). The solid lines correspond to the trajectories generated by the NFxTES.

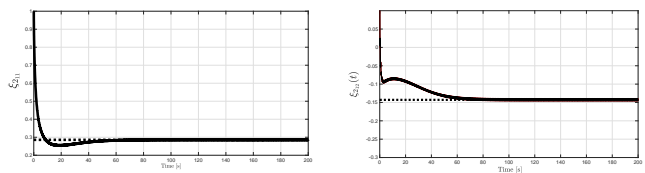


Fig. 3. Evolution in time of the component H_{11}^{-1} of the inverse of the Hessian matrix.

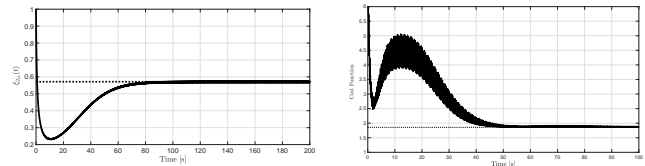


Fig. 4. Evolution in time of the component H_{22}^{-1} of the inverse of the Hessian matrix.

by the NFxTES dynamics and by the classic Newton-based ES dynamics. It can be observed that the NFxTES dynamics exhibit a much better transient performance in terms of less oscillations and faster convergence time to a neighborhood of x^* . On the other hand, Figures 3-4, show the evolution of the components of the state ξ_1 , which correspond to the entries of H^{-1} . As shown in the plots, these states converge to the true values of (28).

To further illustrate the fixed-time convergence property of the NFxTES dynamics, we have also simulated the case where the upper bound on the convergence time is fixed a priori as $T^* = 100$, which can be obtained in the NFxTES dynamics by choosing $k = 0.03085$, $q_1 = 3$, and $q_2 = 1.5$. Figure 5 shows the evolution in time of 50 different trajectories $x(t)$ initialized randomly in the set $[-10, 10] \times [-10, 10]$. As it can be observed, the NFxTES dynamics guarantee convergence to a small neighborhood of x^* before the prescribed time T^* . The simulations used the same parameters $(a, \varepsilon_1, \kappa_i)$ as in Figures 1-4, and ε_2 was selected as 6.25 to guarantee stability.

5. CONCLUSIONS

This paper presented a novel Newton-based extremum seeking controller that achieves fixed-time convergence in

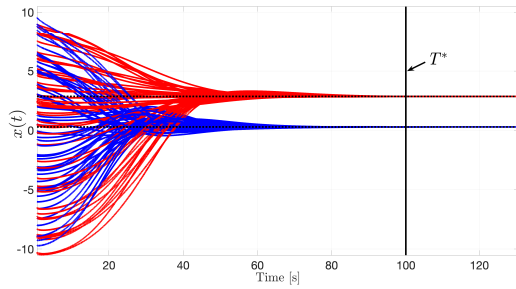


Fig. 5. Evolution in time of several solutions x initialized in a neighborhood of the optimizers. The solid black line indicates the upper bound T^* on the convergence time.

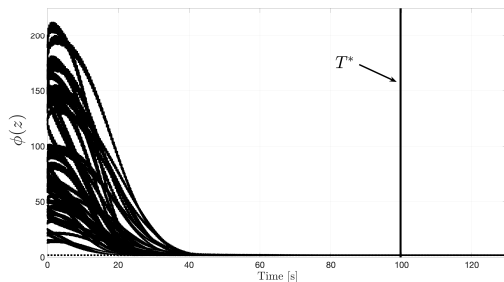


Fig. 6. Evolution in time of 50 trajectories of the cost function $\phi(z(t))$ generated by the 50 solutions x shown in Figure 5. The solid black line indicates the upper bound T^* on the convergence time.

static maps, i.e., the convergence time is bounded by a constant that can be arbitrarily assigned by the designer. The learning dynamics of the extremum seeking algorithm implement a continuous vector field that receives as inputs the estimations of the gradient and the Hessian of the cost function $\phi(z)$, which are obtained by using only measurement of the cost. Local practical convergence in fixed-time was established by using tools from singular perturbation theory and averaging. The advantage of the method in comparison to the traditional Newton-based scheme was illustrated in numerical examples.

REFERENCES

- Alvarez, F., Attouch, H., Bolte, J., and Redont, P. (2002). A second-order gradient-like dissipative dynamical system with hessian-driven damping: Application to optimization and mechanics. *J. Math. Pures Appl.*, 81, 747–779.
- Andrieu, V., Praly, L., and Astolfi, A. (2008). Homogeneous approximation, recursive observer design, and output feedback. *SIAM J. Control Optim.*, 47(4), 1814–1850.
- Ariyur, K.B. and Krstić, M. (2003). *Real-Time Optimization by Extremum-Seeking Control*. Wiley.
- Cruz-Zavala, E., Moreno, J.A., and Fridman, L. (2010). Uniform second-order sliding mode observer for mechanical systems. *Proc. Int. Workshop Variable Struct. Syst.*, 14–19.
- Engel, R. and Kreisselmeier, G. (2002). A continuous-time observer which converges in finite time. *IEEE Transactions on Automatic and Control*, 47, 1202–1204.
- Garg, K. and Panagou, D. (2018). Fixed-time stable gradient-flow schemes: Applications to continuous-time optimization. *arXiv:1808.10474*.
- Ghaffari, A., Krstić, M., and Nešić, D. (2012). Multivariable newton-based extremum seeking. *Automatica*, 48, 1759–1767.
- Ghaffari, A., Krstić, M., and Seshagiri, S. (2014). Power optimization for photovoltaic micro-converters using multivariable gradient-based extremum-seeking. *IEEE Transactions on Control System Technology*, 22(6), 2141–2149.
- Grushkovskaya, V., Durr, H., Ebenbauer, C., and Zuyev, A. (2017). Extremum seeking for time-varying functions using lie bracket approximations. *20th World Congress*, 50(1), 522–5528.
- Guay, M. and Zhang, T. (2003). Adaptive extremum seeking control of nonlinear dynamic systems with parametric uncertainties. *Automatica*, 39, 1283–1293.
- Li, C., Yu, X., Zhou, X., and Rein, W. (2017). A fixed time distributed optimization: A sliding mode perspective. *In Proc. of 43rd Annual Conference of the IEEE Industrial Electronics Society*, 8201–8207.
- Nešić, D., Tan, Y., Moase, W.H., and Manzie, C. (2010). A unifying approach to extremum seeking: Adaptive schemes based on estimation of derivatives. *49th IEEE Conference on Decision and Control*, 4625–4630.
- Oliveira, T., Krstić, M., and Tsubakino, D. (2017). Extremum seeking for static maps with delays. *IEEE Trans. Autom. Control*, 62(4), 1911–1926.
- Polyakov, A. (2012). Nonlinear feedback design for fixed-time stabilization of linear control systems. *IEEE Transactions on Automatic and Control*, 57(8), 2106–2110.
- Poveda, J.I. and Krstić, M. (2020a). Gradient-based fixed-time extremum seeking. *In Proc. of American Control Conference.*, 2838–2843.
- Poveda, J.I. and Krstić, M. (2020b). Non-smooth extremum seeking control with user-prescribed convergence. *IEEE Transactions on Automatic and Control*, provisionally accepted.
- Poveda, J.I. and Li, N. (2021). Robust hybrid zero-order optimization algorithms with acceleration via averaging in time. *Automatica*, 123.
- Poveda, J.I. and Teel, A.R. (2017). A framework for a class of hybrid extremum seeking controllers with dynamic inclusions. *Automatica*, 76, 113–126.
- Rios, H. and Teel, A.R. (2018). A hybrid fixed-time observer for state estimation of linear systems. *Automatica*, 87, 103–112.
- Romero, O. and Benosman, M. (2019). *Finite-Time Convergence of Continuous-Time Optimization Algorithms via Differential Inclusions*. Neurips, to appear.
- Suttner, R. (2019). Extremum seeking control with an adaptive dither signal. *Automatica*, 101, 214–222.
- Tan, Y., Nešić, D., and Mareels, I.M. (2006). On non-local stability properties of extremum seeking control. *Automatica*, 42(6), 889–903.
- Teel, A.R. and Popovic, D. (2001). Solving smooth and nonsmooth multivariable extremum seeking problems by the methods of nonlinear programming. *In proc. of American Control Conference*, 2394–2399.